# A Novel Rotator Glass in Lead(II) Pentanoate: Calorimetric and Spectroscopic Study

**F. J. Martínez Casado,[†] M. Ramos Riesco,[†] A. Sánchez Arenas,[‡] M. V. García Pérez,[†] M. I. Redondo,[†] S. López-Andrés,[§] L. Garrido,[||] and J. A. R. Cheda*,[†]**

*Departamento de Química Física I, Facultad de Ciencias Químicas, Universidad Complutense, 28040 Madrid, Spain, Sección Departamental de Física Aplicada I, Facultad de Veterinaria, Universidad Complutense, 28040 Madrid, Spain, Departamento de Cristalografía y Mineralogía, Facultad de Ciencias Geológicas, Universidad Complutense, 28040 Madrid, Spain, and Departamento de Química Física, Instituto de Ciencia y Tecnología de Polímeros, CSIC, 28006 Madrid, Spain*

*Received: May 29, 2008; Revised Manuscript Received: September 19, 2008*

Lead(II) pentanoate was studied by DSC, XRD, and FTIR and solid state CP/MAS-NMR spectroscopies. A transition from the crystal to the intermediate phase, at $T_{ss} = 328.2 \pm 0.6$ K, with $\Delta_{ss}H = 8.8 \pm 0.1$ kJ·mol$^{-1}$, and a melting at $T_f = 355.6 \pm 0.3$ K, with $\Delta_f H = 12.6 \pm 0.1$ kJ·mol$^{-1}$, were observed on first heating. The thermal and structural behavior of the lead(II) pentanoate shows as a link between those of the shorter and longer members of the previously studied lead(II) alkanoate series. The optical microscopy and FTIR vs temperature studies show structural changes from the crystal to the intermediate phase and its solid state nature. Moreover, X-ray diffraction and C-13 and Pb-207 CP/MAS-NMR studies confirm the *rotator* nature of the intermediate phase in this compound. Two different glass states, one from the isotropic liquid and another from the *rotator* phase, were obtained by quenching at high and low rates, respectively. The glass transition temperatures (measured at 5 K·min$^{-1}$) were 322.9 and 275.7K, respectively.

## 1. Introduction

The lead compounds are particularly relevant in the coordination chemistry studies of heavy *p*-block elements. Lead compounds with coordination numbers from 2 to 12 are well-known, with 2, 4, and 6 being the most common ones.[1] Conspicuously, the lead compounds with *coordination number* 4 or 6 do not exhibit expected (*standard*) tetrahedral or octahedral geometries. The establishment of the coordination number of the metal and, therefore, its coordination geometry is difficult to obtain.[2] Furthermore, despite the large body of work already published, much remains to be discovered in the field of the lead coordination chemistry.

The lead(II) alkanoate series ($Pb(Cn)_2$, where *n* is the number of carbon atoms) has been studied by several authors. Members with $n \geq 6$[3−9] have been more widely studied because of their interest as mesogens. The latter present *polymesomorphism*, an intermediate phase characterized recently as a *rotator* mesophase,[10] followed by a *smectic-A-like* (or *neat*) liquid crystal phase (only members with $6 \leq n \leq 12$). The shortest members of the series (from acetate to butanoate)[11] show only a melting to the isotropic liquid from the crystal phase, and easily form *glass states*.[9] In fact, metal acetate systems (pure or their binary mixtures) show a strong tendency to form glasses.[12−14]

$Pb(C7)_2$ is the only member of the lead(II) alkanoates series for which a complete structure determination by single crystal XRD at room temperature has been published.[15] The following structural features characterize the structure:

- A *bilayered arrangement* with a lead(II) and carboxylate *ionic* layer and *all-trans* alkyl chain *lipidic* alternating layers. The chains are held together by *van der Waals* interactions along the *chain* direction, whereas the C−C−C planes are arranged following a *herringbone* type distribution.

- A *hemidirected octahedral* geometry for the O environment around the Pb atoms[1,15] in response to the stereochemically active $6s^2$ lone electron pair.

- Two types of carboxylates at one end of the alkyl chains: *only-chelating* and *bridging-chelating*, at 50 %.

Our experimental and simulated XRD study of the unit-cell structures[10,11] on shorter and longer members showed that they are isostructural with $Pb(C7)_2$, in the crystal phase at room temperature.

To our knowledge, there is no information on the $Pb(C5)_2$ member in the literature. The difficulties to synthesize and purify this compound along with its complicated thermal behavior (as described in this work) may be the reason for this lack of data. As shown below, $Pb(C5)_2$ behaves midway between the long and short members: the compound presents a *crystal*-to-*rotator* transition and a melting (as the long members, $n \geq 13$) and a complex vitreous behavior (as the short ones, $n \leq 4$).

Apart from the well known *glass state* (amorphous solid state quenched from the isotropic liquid), other glasses[16,17] are also possible: *plastic crystal glass*[18] (positional order−frozen orientational disorder glass) and *liquid crystal glass*[19] (orientational order−frozen positional disorder glass). The *condis glass*[20] (positional and orientational order−frozen internal conformational disordered glass) is another poorly studied glass. From a theoretical point of view, the formation of a *rotator glass* from the *rotator* phase could be possible. This may imply a state where the alkyl chain rotation movement of the *rotator* phase is frozen, and the *all-trans* planes of the chains remain in static random orientation, maintaining their positional order (hexagonal or *pseudo*-hexagonal arrangement). We show here the

* Corresponding author. Phone: +91-3944306. Fax: +91-3944135. E-mail: cheda@quim.ucm.es.
[†] Departamento de Química Física I, Facultad de Ciencias Químicas, Universidad Complutense.
[‡] Sección Departamental de Física Aplicada I, Facultad de Veterinaria, Universidad Complutense.
[§] Departamento de Cristalografía y Mineralogía, Facultad de Ciencias Geológicas, Universidad Complutense.
[||] CSIC.

10.1021/jp804757n CCC: $40.75 
Published on Web 11/26/2008

formation of this last, uncommon glass, for lead(II) pentanoate. To our knowledge, this *rotator glass* is reported for the first time.

It is worth mentioning here that lead poisoning remains one of the most common environmental health hazards, which adds interest to the search for powerful and selective lead binding materials and ligand systems.[21] In fact, no effective oral chelators are known to be used in therapeutic treatment of lead poisoning. Another interesting aspect of lead(II) pentanoate is the formation of passive film on lead surfaces[15] that can be used as a corrosion inhibitor in conservation of artwork made up of lead. Besides, $Pb(C5)_2$ is a nonvolatile ionic solvent, since it melts below 100 °C, being an *ionic liquid* (organic salt which melts under 100 °C with interest as ionic solvent).[22,23]

## 2. Experimental Section

**Sample Preparation.** The usual method[9] of synthesis (used to obtain the longer members of the lead(II) alkanoates series) was not successful for $Pb(C5)_2$. Consequently, this compound was prepared by a reaction between pentanoic acid (Fluka, ≥99 %) and lead(II) oxide (Aldrich, >99 %) in ethanol (Carlo Erba, >99.7 %). The obtained salt was recrystallized twice in ethanol and vacuum dried. This method is the same as that employed for the synthesis of $Pb(C3)_2$ and $Pb(C4)_2$. The mol percent purity obtained by the DSC fractional technique is 99.47 %. No traces of pentanoic acid (one of the possible impurities) were detected by the other techniques used (e.g., FTIR or titration).

**Differential Scanning Calorimetry.** A TA Instruments DSC Model Q10 was used in this work. Tightly sealed aluminum volatile pans (in $N_2$(g) atmosphere) were used to scan at different heating rates (5 $K \cdot min^{-1}$, in dry nitrogen atmosphere at a gas flow of about 50 $mL \cdot min^{-1}$). An MT5 Mettler microbalance was used to weigh the about 10 mg samples (error ±0.001 mg). The calorimeter was calibrated for temperature using standard samples of In and Sn, supplied by TA (purity >99.999 % and >99.9 %, respectively), and of benzoic acid (purity >99.97 %), supplied by the former NBS (lot 39i). Regarding enthalpy, we calibrated using the standards of In and Sn described above.

**X-ray Diffraction.** XRD measurements were carried out with a Philips X'Pert PRO MPD X-ray diffractometer with vertical goniometer $\theta/\theta$ (Cu $K_{\alpha 1}$ radiation, 1.540 56 Å, Ni filter), X'Celerator detector, equipped with a high-temperature chamber Anton Paar HTK1200. The in situ XRD area was scanned from $2\theta = 2-70°$ at several temperatures in the range from 25 to 95 °C during the heating and the cooling, at a rate of 3 °C/min.

**FTIR Spectroscopy.** Mid-infrared spectra of Pb(II) pentanoate in KBr pellets and powders between two pure KBr pellets were recorded at a resolution of 4 $cm^{-1}$ in a Nicolet Magna 750 FTIR spectrometer. No significant differences between the spectra obtained by both procedures were observed. A commercial variable temperature cell, SPECAC VTL-2, adapted for solid samples was employed to obtain IR spectra at different temperatures.

**C-13 and Pb-207 CP/MAS-NMR.** Solid state C-13 and Pb-207 NMR measurements were performed in a Bruker Avance 400 spectrometer (Bruker Analytik GmbH Karlsrube, Germany) equipped with a 89 mm wide bore and a 9.4 T superconducting magnet (C-13 and Pb-207 Larmor frequencies at 100.61 and 83.71 MHz, respectively). Powdered samples were placed in 4 mm zirconia rotors (about 60 mg of sample). All reported data were acquired at two temperatures, first at 296 ± 0.1 K and then after thermal equilibrium was reached at 343 ± 0.1 K. We used a standard Bruker double resonance 4 mm cross-polarization (CP)/magic angle spinning (MAS) NMR probe head

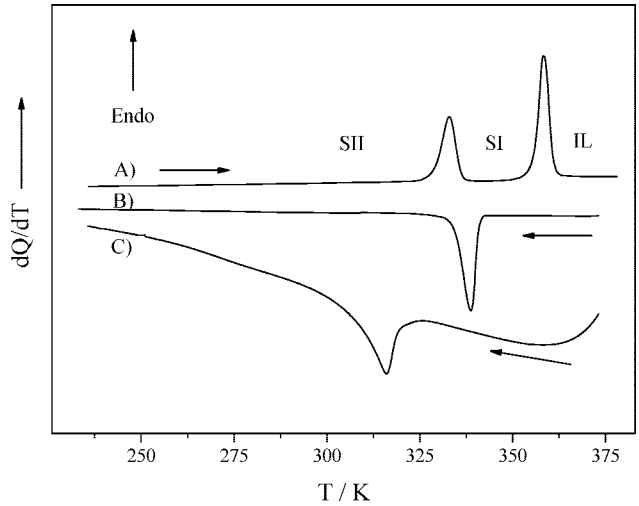


**Figure 1.** Thermograms of $Pb(C5)_2$: (A) first heating at 5 $K \cdot min^{-1}$; (B) cooling at 5 $K \cdot min^{-1}$; (C) cooling fast, at approximately 40 $K \cdot min^{-1}$.

using a 90° C-13 pulse length of 4.2 μs. The C-13 spectra were acquired with 1 ms CP contact time, 5 s recycle delay, MAS spinning rates of 6.5 kHz, and 1000 transients. High-power proton decoupling of 75 kHz was used. The NMR spectra were evaluated with the spectrometer manufacture's software package XWIN-NMR. All free-induction decays were subjected to standard Fourier transformation with 5 Hz line broadening and phasing. The chemical shifts were externally referenced to adamantane (29.5 ppm) secondary to TMS (0.0 ppm).

The Pb-207 NMR spectra were acquired with 4 ms CP contact time, 10 s recycle delay, MAS spinning rates of between 4.0 and 9.0 kHz, and 3000 to 12 000 transients. High-power proton decoupling of 75 kHz was used, and the NMR spectra were also evaluated with XWIN-NMR. All free-induction decays were subjected to standard Fourier transformation with 240 Hz line broadening and phasing. The chemical shifts were externally referenced to tetraphenyllead(IV) (−135 ppm).[24]

**Optical Microscopy.** To identify the nature of the phases (solid or liquid), we used a Carl Zeiss-Jena polarizing optical microscope, model pol-30-G0527, equipped with a LINKAM hot stage, model THMS600, connected to a LINKAM programmable temperature controller, model TMS94.

## 3. Results

**Differential Scanning Calorimetry (DSC).** The first heating and two cooling thermograms of lead(II) pentanoate are shown in Figure 1. Two transitions are observed on heating (Figure 1A), which correspond to a solid-to-solid (SII-to-SI) transition and to the melting process (SI-to-isotropic liquid, IL). Depending on the cooling rate, the thermal behavior may strongly differ in the second heating. At the slow cooling rate of 5 $K \cdot min^{-1}$ (Figure 1B), only one exothermic peak (with the same area of the peak of melting) appears, which corresponds with the solidification of IL to SI. The second peak does not appear at any temperature. In fact, when heating the cooled sample again, the thermogram represented in Figure 2A shows a glass transition (Tg1) at 322.9 K (see Scheme 1). Thus, a glass state (GI) of the SI solid phase should be formed below room temperature. On the other hand, when cooling faster at 40 $K \cdot min^{-1}$ (Figure 1C), a more undercooled single peak is observed. The evaluated area of this peak (normalized for the different rates) is smaller than that observed during the slow cooling. This indicates that only a part of the IL was converted

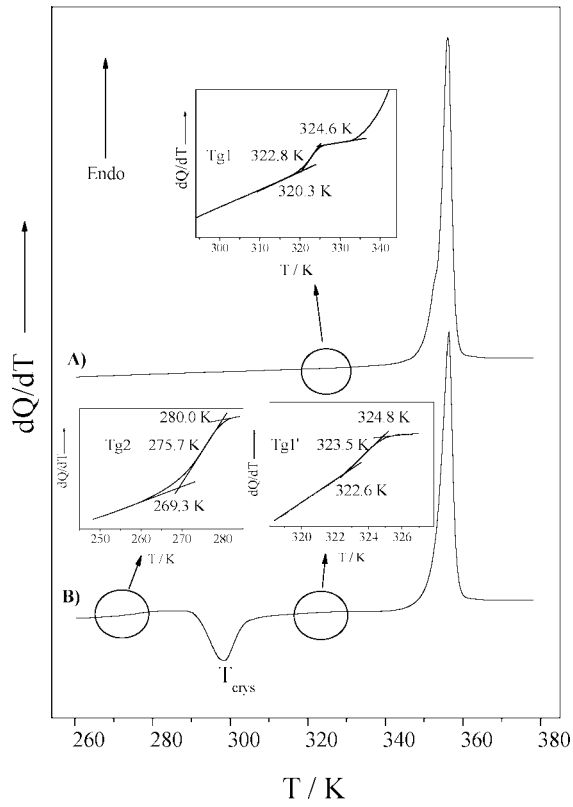


**Figure 2.** Second heating thermograms of $Pb(C5)_2$, after cooling from the isotropic liquid.

**SCHEME 1**

$$GI \xrightarrow{Tg1} SI \xrightarrow{T_{SI\text{-}IL}} IL$$

**SCHEME 2**

$$GII\,(+GI) \xrightarrow{Tg2} IL'(+GI) \xrightarrow{T_{crys}} GI \xrightarrow{Tg1'} SI \xrightarrow{T_{SI\text{-}IL}} IL$$

into SI. Since a second peak does not appear on further cooling of the sample, a mixture of two glass states (GI and GII) must have formed. This is confirmed in the corresponding second heating thermogram (Figure 2B), where a Tg2 at 275.7 K (corresponding to the common glass state transition) and a Tg1 at 323.5 K (corresponding to the SI glass (GI) transition) are observed. The exothermic peak, at $T_{crys}$, appearing between these two glass transitions is due to the crystallization of the metastable isotropic liquid to the SI glass phase (GI) (see Scheme 2). A 35% of GII in the mixture of glass states GII and GI formed on cooling was calculated by comparison of the crystallization and melting enthalpies (4.3 and 12.4 $kJ \cdot mol^{-1}$, respectively).

The thermal functions (temperatures, enthalpies, and entropies of transition) of $Pb(C5)_2$, for the first and the two types of second heatings, are summarized in Table 1, in which the glass transition temperatures (measured at 5 $K \cdot min^{-1}$) are also included.

The sample recovers to its initial behavior (first heating thermogram) after waiting at room temperature for about 2 months, thus indicating that this is the stable thermal behavior.

With the aim of studying the kinetics of these glass transitions, DSC traces of both quenching phenomena were registered at different heating rates (see Figures 3 and 4). The corresponding glass transition (Tg2 and Tg1) and crystallization temperatures ($T_{crys}$) are shown in Table 2.

**Optical Microscopy.** A "droplet" experiment[25] was performed on $Pb(C5)_2$ with a polarizing light microscope. This

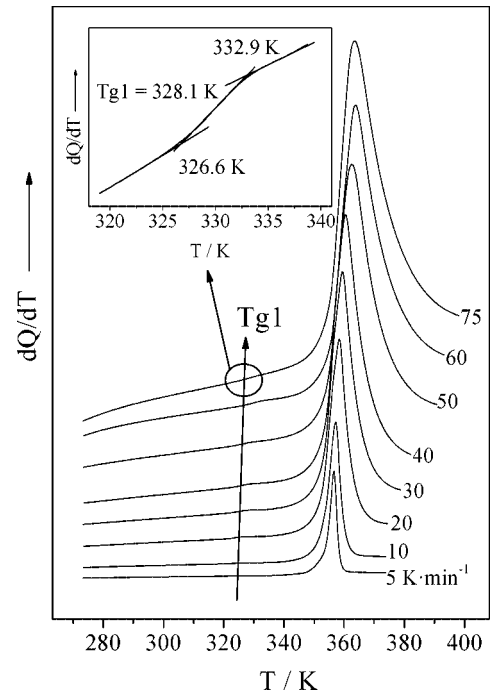


**Figure 3.** Thermograms obtained after slow quenching from the isotropic liquid, registered at the specified heating rates.

**TABLE 1: Thermal Functions of $Pb(C5)_2$ (a) in the First Heating, (b) Second (and Following) Heatings after a Slow Quenching, and (c) Second (and Following) Heatings after a Fast Quenching**

| | transition | $T$/K | $\Delta_{trs}H$/kJ·mol$^{-1}$ | $\Delta_{trs}S$/J·K$^{-1}$·mol$^{-1}$ |
|---|---|---|---|---|
| (a) | SII−SI | 328.2 ± 0.6 | 8.8 ± 0.1 | 26.8 ± 0.4 |
| | SI−IL | 355.6 ± 0.3 | 12.6 ± 0.1 | 35.3 ± 0.3 |
| (b) | Tg1 | 322.9 ± 0.5 | | |
| | SI−IL | 354.3 ± 0.4 | 12.3 ± 0.3 | 34.8 ± 0.8 |
| (c) | Tg2 | 275.7 ± 0.5 | | |
| | Tg1′ | 323.5 ± 0.5 | | |
| | SI−IL | 354.5 ± 0.6 | 12.4 ± 0.3 | 35.1 ± 0.8 |

experiment consisted of the observation of small crystalline particles suspended in mineral oil (Brookfield 30000, viscosity 29920, in which the material is insoluble) at different temperatures. Spherical droplets are formed only if fluid phases appear, showing birefringence only in the case of liquid crystal phases. Isotropic spherical drops formed above 355.6 K (IL) disappeared when the *intermediate* (SI) phase was reached on cooling, and irregular shaped birefringent particles were formed instead. This confirms the solid nature of this phase. Moreover, the pure sample does not shear under stress during optical observations. For all of these reasons, an ordered *liquid crystal* phase was ruled out for the SI phase.

**X-ray Diffraction.** A simulation of the unit cell for $Pb(C5)_2$ (Figure 5A) was done using the data of the $Pb(C7)_2$ single crystal structure with the Mercury software.[15] The process consisted of shortening the *c* parameter by twice the $CH_2$ group length in the *trans* position, creating a CIF file with the atom coordinates. The comparison between the experimental and simulated (from this estimated structure) powder diffraction patterns showed excellent agreement (Figure 5B), confirming that the $Pb(C5)_2$ and $Pb(C7)_2$ are isostructural, thus maintaining the P-1 triclinic structure. The cell parameters proposed for the $Pb(C5)_2$ are shown in Table 3.

Two types of chains with carboxylate groups, either *only-chelating* or *bridging-chelating*, and the *all-trans* carbon planes

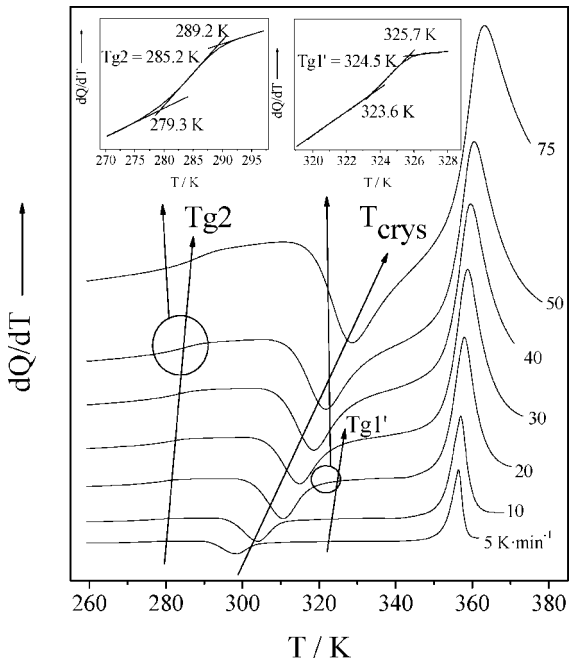


**Figure 4.** Thermograms obtained after a fast quenching (20−30 $K \cdot min^{-1}$) from the isotropic liquid, registered at the specified heating rates.

**TABLE 2: Temperatures of the Different Glass Transitions and Crystallization after Slow Quenching (Tg1) and after Fast Quenching (Tg2, $T_{crys}$, and Tg1′), Measured at Different Heating Rates (The Error in the Temperatures Is ±0.5 K)**

| heating rate/$K \cdot min^{-1}$ | Tg1 | Tg2 | $T_{crys}$ | Tg1′ |
|---|---|---|---|---|
| 5 | 322.9 | 275.7 | 298.5 | 323.5 |
| 10 | 323.3 | 277.4 | 304.0 | 323.8 |
| 20 | 323.8 | 279.2 | 310.7 | 324.5 |
| 30 | 324.8 | 281.8 | 314.9 | 325.9 |
| 40 | 325.4 | 283.3 | 318.5 | |
| 50 | 326.5 | 285.2 | 321.8 | |
| 60 | 326.8 | | | |
| 75 | 328.1 | 289.7 | 328.6 | |

with a *herringbone* orientation are observed (Figure 5A). This solid SII structure is common to all of the $Pb(Cn)_2$ members. The experimental powder XRD *d-spacing* (00*l*) data on the two solid phases (SII and SI) for $Pb(C5)_2$ measured as a function of temperature are represented in Figure 6A. This parameter decreases when passing from SII to SI. In addition, the value of *d* for SI remains constant when cooling the sample to room temperature, thus confirming the formation of the vitreous state (GI) of this phase.

The $Pb(C5)_2$ 00*l d*-spacings fit within the general behavior of the whole series (Figure 6B). The *d*-spacing decreases from SII to SI in an amount which is independent of the number of carbon atoms. Moreover, the *d-spacings* increase linearly with *n* with the same slope of 2.47 Å/*n* for both ordered *crystal* (SII) and *intermediate* (SI) phases.

**FTIR Spectroscopy.** FTIR spectra of $Pb(C5)_2$ were recorded from 298 to 400 K on heating and from this temperature to 298 K on cooling. Figure 7 shows the room temperature spectrum of this compound. The high-frequency region from 2800 to 3000 $cm^{-1}$ corresponds to the C−H stretching modes. Besides, the region from 600 to 1600 $cm^{-1}$ displays the stretching modes of the carboxylate group, bending modes of the $CH_3$ group, and the scissoring, rocking, wagging, and twisting modes of the methylene groups. Bands due to vibrations of the Pb−O bonds are also observed in the low-

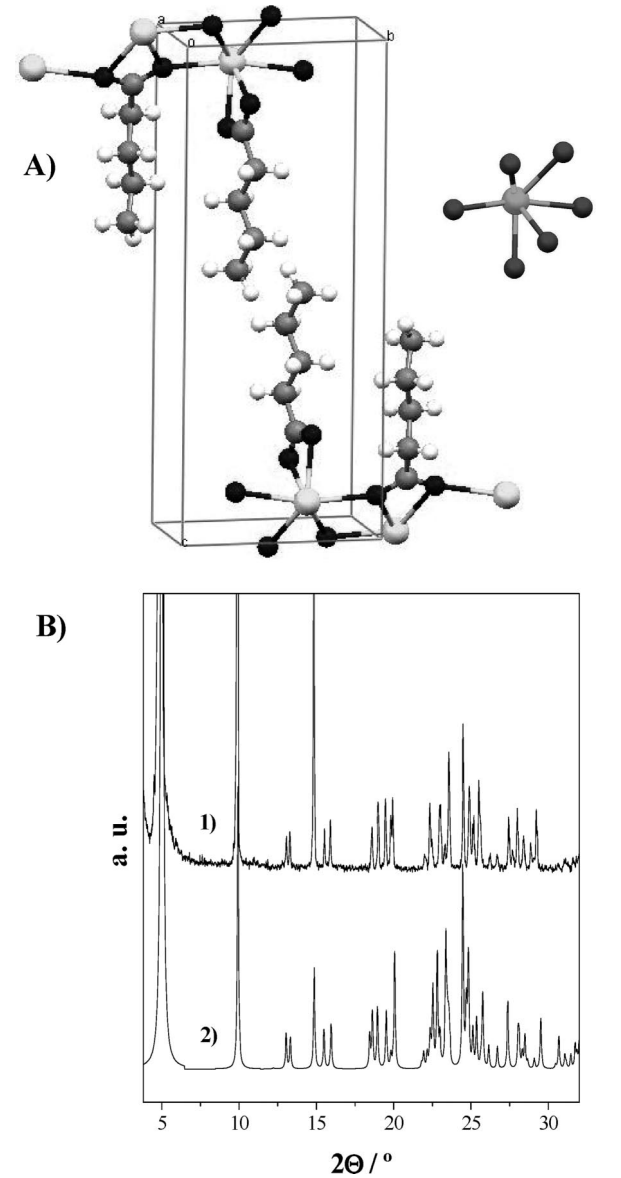


**Figure 5.** (A) Simulated unit cell for the $Pb(C5)_2$ (left) and *hemidirected octahedral* coordination of lead(II) (right). (B) Comparison between the experimental (1) and the simulated (2) powder diffraction patterns of $Pb(C5)_2$.

**TABLE 3: Parameters for the Simulated Unit Cell of the $Pb(C5)_2$ in the SII Phase**

| *a*/Å | *b*/Å | *c*/Å | α/deg | *β*/deg | *γ*/deg |
|---|---|---|---|---|---|
| 4.857 | 7.305 | 18.093 | 91.61 | 95.66 | 90.99 |

frequency region between 400 and 600 $cm^{-1}$. The anti-symmetric ($\nu_{as}$ $COO^-$) stretching vibration of the carboxylate group can be observed in the crystal at room temperature (SII) at 1507 $cm^{-1}$ (with a shoulder at about 1527 $cm^{-1}$). The presence of these two bands is indicative of two coordination types of the carboxylate groups to the Pb atoms; however, no splitting is observed in the 1406 $cm^{-1}$ band assigned to the symmetric ($\nu_s$ $COO^-$) mode.

Temperature evolution of the infrared spectra is shown in Figure 8, where it is observed that the anti-symmetric stretching vibration of $CH_3$ ($\nu_{as}$ ($CH_3$)) is split into two bands at 2962 and 2954 $cm^{-1}$ that merge into one band from 328 K (SI) until the liquid phase (Figure 8A). The $\nu_{as}$ ($CH_3$) anti-symmetric vibration is degenerate and appears as a single band when the methyl

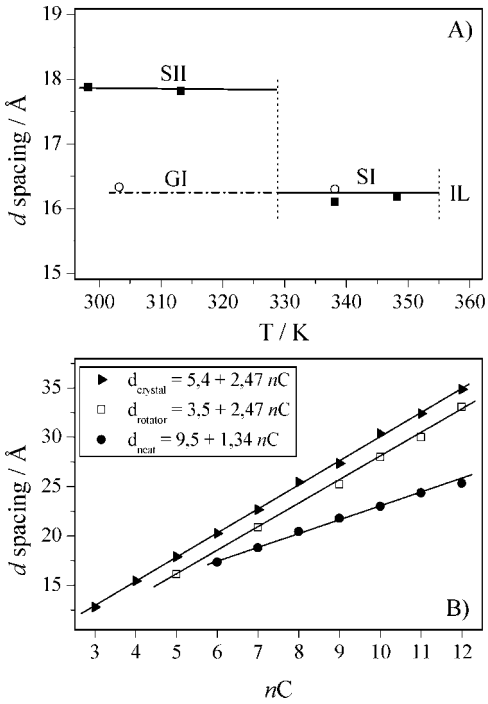


**Figure 6.** (A) *d-Spacing* vs temperature for the $Pb(C5)_2$ phases (■, on heating; ○, on cooling). $S_{II}$, ordered crystal; $S_I$, *rotator* phase; $G_I$, $S_I$, *glass* state; IL, isotropic liquid. (B) *d-Spacings* vs alkyl chain number of carbons (*n*), for the following: right-pointing solid triangle, crystal phase; □, *rotator* phase; ●; neat phase.

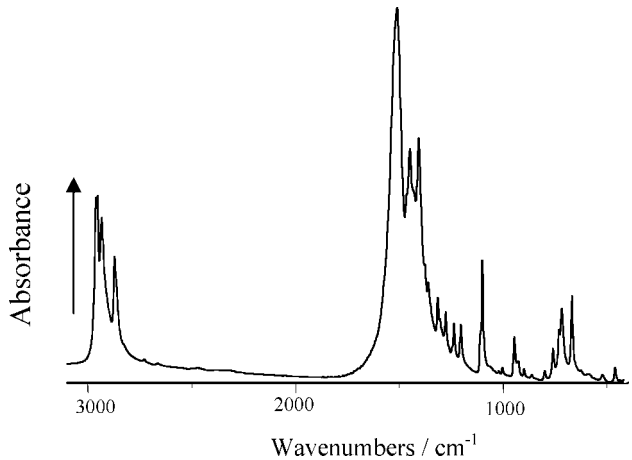


**Figure 7.** FTIR spectrum of $Pb(C5)_2$ at room temperature.

group is in a symmetric environment. Given that two bands are observed in $Pb(C5)_2$, we can deduce that the terminal alkyl chains interact at low temperature, breaking the degeneration of the vibration. At temperatures higher than 328 K, only one band is observed. This feature could be due either to a decrease of the interactions by a crystal expansion or to a free rotation of the methyl group.

Remarkable changes with temperature are observed in the carboxylate region (Figure 8B). The ($\nu_{as}$ $COO^-$) *stretching* vibration observed at 1507 $cm^{-1}$ and the shoulder at 1527 $cm^{-1}$ in the SII phase merge into a unique band at 1537 $cm^{-1}$ in SI. This band remains up to the moment the liquid phase is reached. A set of regularly spaced bands is observed between 1350 and 1150 $cm^{-1}$, in both solid phases. This region corresponds to the $CH_2$ *wagging* modes. In compounds with a large alkyl chain and an *all-trans* conformation, a number of *wagging* progression bands (depending on the chain length) are displayed.[26] Three [(*n*+1)/2] of these bands are observed in this compound. When temperature rises, from the SII to the SI phase, some frequency shifts and intensity variations of these bands occur, and the development of a new band at around 1306 $cm^{-1}$ (ascribed to localized $g^{\pm}tg^{\mp}$ (*kink*) sequences in the alkyl chain)[27] is observed.

The peak at 717 $cm^{-1}$ in the room temperature crystal (SII) (Figure 8C) is assigned to the $CH_2$ *rocking* vibration in *all-trans* chains. At the SII-to-SI transition temperature, this band shifts to 708 $cm^{-1}$ and becomes broader and weaker, and simultaneously, the band at about 760 $cm^{-1}$ (characteristic of $CH_2$ *rocking* vibrations in disordered chains) becomes stronger. The frequency and width of the $\delta$ ($COO^-$) vibration at 668 $cm^{-1}$ also changes with temperature, thus indicating that structural changes in the ionic layer from SII to SI are taking place.

All of these changes in the bands are compatible with the hypothesis suggesting that the intermediate solid phase (SI) is a *rotator* phase. This would be the result of the existence of only one type of carboxylate and alkyl chains, where the rotation allows certain conformational defects.[28] This explains also the intensity decrease of the $CH_2$ *wagging* progression bands, the changes in the frequency of the *rocking* vibration, and the presence of *kink* defect bands.

**Nuclear Magnetic Resonance (C-13 and Pb-207).** Figure 9 illustrates the C-13 CP/MAS-NMR spectra of the crystal (SII) at 296 K, *rotator* (SI) at 343 K and solid (GI) at 296 K from 343 K phases of $Pb(C5)_2$. Five groups of signals corresponding to the five carbon atoms in the compound, from the carboxylate centered at ~183 ppm to the methyl group centered at ~14 ppm, are observed.

All of the bands appear as doublets with the approximate same area in the spectrum taken on the crystal (SII). In the spectrum corresponding to the *rotator* phase (SI), the doublets associated to the carbons at the end of the chain (methyl and methylene) collapse into a singlet and multiplicity increases for the rest of the carbons. The subsequent cooling of the sample freezes the disorder introduced by the thermal changes and leads to a more complex spectrum with increased multiplicity in all peaks.

Figure 10 shows the Pb-207 spectra corresponding to the *crystal* (A) and *rotator* (B) phases acquired at 296 and 343 K, respectively. The spectra exhibit the characteristic peak patterns associated to these lead compounds[29] with a central peak at −(638 ± 5) ppm (spectrum acquired at 296 K) and spinning side bands at $\pm n\nu_r$ (spinning rate 6.5 kHz or 79.6 ppm). It should be noted that in the figure partial $^{207}Pb$ spectra are shown; the full spectral width extends over 1500 ppm, exceeding the maximum bandwidth available in our spectrometer. The shape of the spectrum envelope changes at 343 K, and the central peak shifts to −555 ppm. In both cases, the peak assignment was accomplished by comparing the profiles of two or three spectra acquired with different spinning rates. At high temperature, the increased molecular mobility causes a loss of cross-polarization efficiency, leading to spectra with poor signal-to-noise ratio which hampers adequate phasing of spectrum B and the assignment of individual parameters to each peak. Despite the uncertainty of these results, a splitting of the central band is noticeable, particularly in the region of the spectrum with high-intensity peaks (between −700 and −1000 ppm, approximately). This suggests a change in the environment of the $Pb^{2+}$ ions when increasing the temperature from the SII to the SI phase. The spectrum obtained at 296 K after cooling from 343 K (data not shown) exhibits only singlets (Figure 10A) but with the central band located at an intermediate frequency, between −555 and −638 ppm.

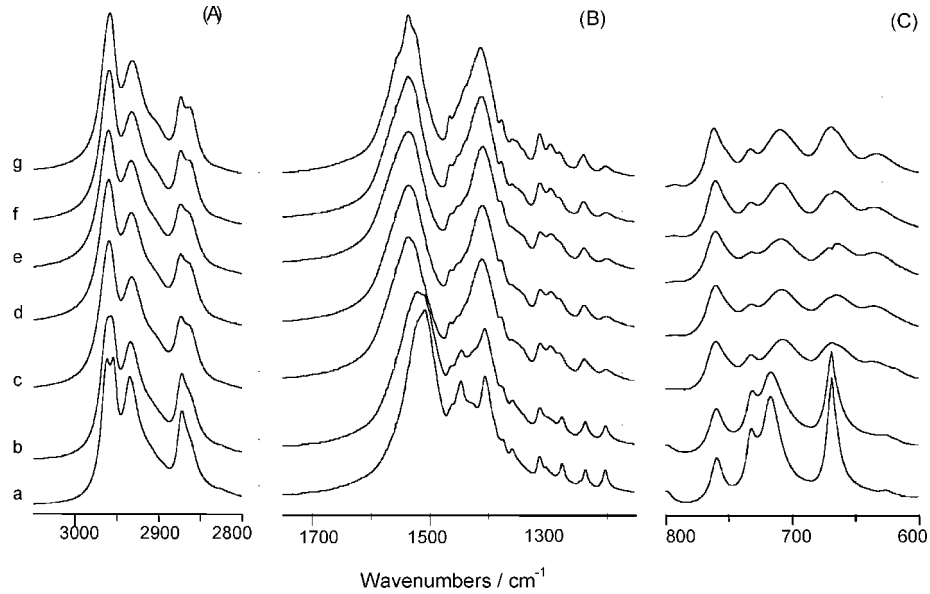


**Figure 8.** FTIR spectra of $Pb(C5)_2$ at (a) 298 K, (b) 318 K, (c) 328 K, (d) 348 K, (e) 368 K, (f) 318 K (immediately after melting), and (g) 298 K (3 days after melting).

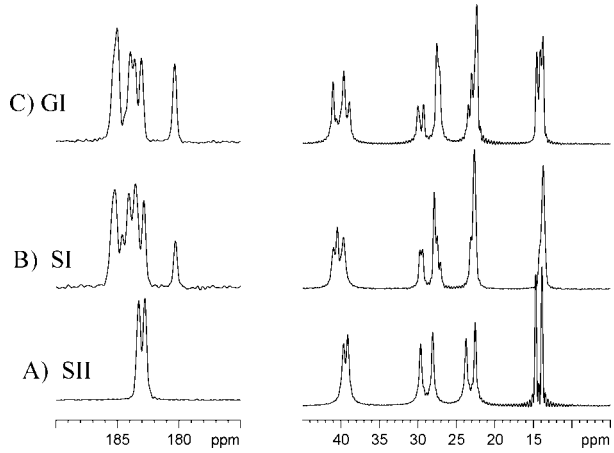


**Figure 9.** C-13 CP/MAS-NMR spectra of $Pb(C5)_2$: (A) crystalline phase (SII) at room temperature; (B) *rotator* phase (SI) at 343 K; (C) solidified after being melted (GI) at room temperature.

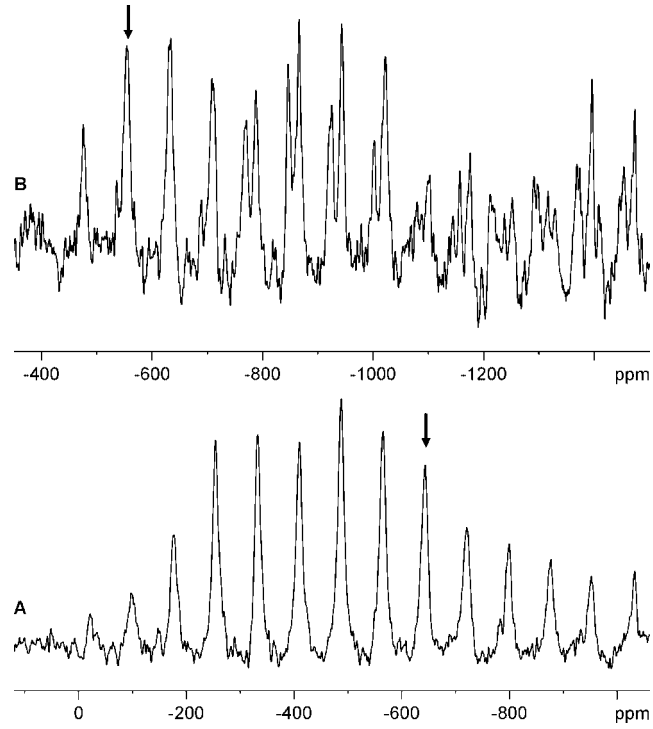


**Figure 10.** Pb-207 CP/MAS-NMR spectra of $Pb(C5)_2$: (A) crystalline phase (SII) at room temperature; (B) *rotator* phase (SI) at 343 K. The central peaks are indicated with arrows.

## 4. Discussion

On the basis of the above examined experimental results, the intermediate solid phase appearing in $Pb(C5)_2$ has been assigned to a *rotator* phase similar to the one present in lead(II) alkanoates with $n \geq 6$.[10] In addition, also a *rotator glass* phase (GI) has been detected.

**Rotator Phase (SI) and Rotator Glass (GI).** Although the *rotator* phase had been widely studied for hydrocarbons[30−32] or alkyl ammonium salts,[33,34] this phase has been only recently reported in the lead(II) alkanoates.[10] The "*droplet*" experiment described previously in section 3 rules out the possibility of considering the *intermediate* phase (SI) as a type of *smectic* B (or G), whose structure is also *hexagonal* and the molecules also rotate.[35] In addition, the XRD information about the *d-spacing*s is crucial for the characterization of SI. As shown in Figure 6B, the *d*-spacings vary with the same slope of 2.47 Å/*n* in both solid phases. This slope corresponds to the contribution of two $CH_2$ groups to the *d-spacing*.

Considering the generally accepted values of 1.53 Å for the C−C bond length and 112° for the C−C−C angle,[36,37] the increase in the *d*-spacing per methylene group (in a bilayered compound with *all-trans* alkyl chains perpendicular to the layers) should be 2.54 Å/*n*.

Thus, the tilt angle ($\theta$) between the chains and the ionic layers would be $\theta = \arccos(2.47/2.54)$, that is, 14° for both the SII and SI phases. Taking all of these considerations into account, the existence of either a *condis* or a *liquid crystal* phase (for the SI structure) should be excluded as a possibility.

Figure 6A shows the direct relationship between SI and GI phases, which have the same values for the *d*-spacing. Therefore, after quenching, the SI positional order is maintained, whereas the SI chain rotation is frozen. Thus, a rotator glass state has been obtained.

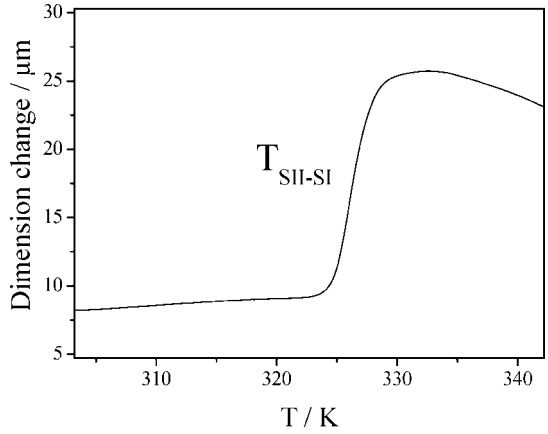


**Figure 11.** TMA plot of $Pb(C5)_2$, showing the discontinuity at the temperature of transition $T_{SII-SI}$.

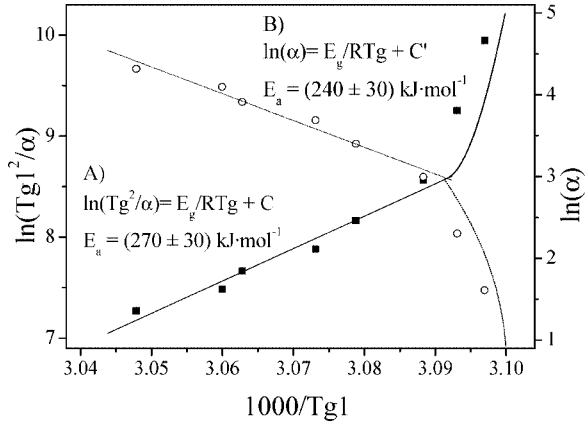


**Figure 12.** Kissinger's (A) and Ozawa's (B) plots for Tg1 (GI-to-SI).

**TABLE 4: Activation Energy ($E_a$) of the Two Glass Transitions (GII−IL′ and IL′−GI) and the Crystallization Process (IL′−GI), from Kissinger's and Ozawa's Equations**

| kinetic process | Kissinger $E_a$/kJ·mol$^{-1}$ | Ozawa $E_a$/kJ·mol$^{-1}$ |
|---|---|---|
| GII−IL′ (Tg2) | 80 ± 8 | 99 ± 6 |
| IL′−GI ($T_{crys}$) | 56 ± 3 | 62 ± 3 |
| GI−SI (Tg1) | 270 ± 30 | 240 ± 30 |

The FTIR analysis shows some structural changes between the SII and SI phases. The carboxylate *stretching* vibration collapses into one band in the SI phase, thus indicating a Pb(II) coordination change, possibly from *bridging-chelating* to *only-chelating* in the SII-to-SI transition. This would explain the decrease observed in the SI layer thickness (Figure 6A). The *anti-symmetric* stretching vibrations of $CH_3$ are split into two bands in SII, whereas they merge into a single one in SI. This agrees with the existence of only one kind of methyl group in the *rotator* phase, as shown by the C-13 NMR results. The *wagging* progression bands (typical of *all-trans* conformation) do not disappear in SI, showing only some frequency shifts and intensity variations. Furthermore, the observed band at 1306 cm$^{-1}$ in SI shows the formation of localized $g^{\pm}tg^{\mp}$ (*kink*) sequences, typical of *rotator* phases.[28] The FTIR spectrum of GI (obtained by cooling the sample after melting) is exactly the same as that of the SI phase (see Figure 8), confirming once more the similar structure of both phases.

Figure 9A shows the SII crystal C-13 MAS-NMR spectra, where the carbon split into doublets corresponds to the two types of chains: two different carboxylates with their herringbone oriented alkyl chain planes (Figure 5A).

The spectrum corresponding to the *rotator* phase (Figure 9B) shows the collapse of the doublets associated with carbons 4 (methylene) and 5 (methyl) at the end of the chain, which can be attributed to an increase of their molecular mobility. The increase is not sufficient to produce a similar effect on the peaks of the other carbons but causes the splitting of the corresponding peaks into multiple lines. The change observed in the carboxylate carbon peak from a doublet (in SII) to six peaks (in SI) suggests the presence of a molecular structure with six nonequivalent positions (possibility of pseudo-hexagonal arrangement).

The GI glass C-13 MAS-NMR spectra exhibit a more complicated pattern, most likely due to the freezing of a diverse set of molecular conformations, especially for the methyl and $\gamma$-methylene groups. This also enhances the six signals for the C atom of the carboxylate, as observed in SI. This fact suggests a disorder in the orientation of the *all-trans* chains planes which lose the *herringbone* structure, as one may expect in a *rotator glass* phase (GI). As inferred from the FTIR spectroscopy, only some defects (like *end gauche* or *kink*)[28] are possible in the alkyl chains. However, these defects are not common: less than 10 % would present a *gauche* defect, with the rest of the carbons remaining in the *trans* configuration, as proved by simulation and experimental studies.[38,39]

These results are confirmed by the Pb-207 CP/MAS-NMR findings (Figure 10) that suggest a change from a high-symmetry SII crystal structure to a somewhat less ordered SI one. As expected from the crystalline structure, only one environment (one peak) is detected for the Pb atoms in the SII phase (at room temperature, Figure 10A), and all of the lead(II) atoms have a *hemidirected octahedral* coordination. However, the spectra for the SI phase show two peaks, that is, two types of Pb atoms (Figure 10B). This suggests a probable change in the lead(II) coordination number associated with a polymorphic change from a triclinic to a rectangular or *pseudo*-hexagonal 2D lateral packing of the alkyl chains. The results for SI are the same as those for GI, showing a relationship between the *rotator* and *rotator glass* phases (SI and GI, respectively).

As observed in all of the known cases, the change from a totally crystalline to a *rotator* phase always involves an increase of the unit-cell volume, allowing more space for the alkyl chains to rotate around their molecular axis. This expansion in the hydrocarbons[30−32] occurs in the three space directions, but there are series (e.g., the dimethyl pyrrolidinium halides,[40] the alkyl ammonium halides,[41,42] or the lead(II) alkanoates[10]) in which a contraction of the *c* parameter is detected at the transition to the *rotator* phase (whereas the lattice volume increases). Dilatometric measurements were carried out by TMA (see Figure 11) to check the density decrease (increase of the unit-cell volume) in the $Pb(C5)_2$ *rotator* phase, and the same results as those for the longer lead(II) alkanoates[10] were obtained. This means that the contraction of the *c* parameter implies a larger expansion in the *x*−*y* plane (*a* and *b* parameters of the unit cell), thus facilitating the rotation around the molecular axis. Dilatometry measurements made by Bazuin et al.[3] in $Pb(C10)_2$ show that the area per polar head (*S*) increases from 19 Å$^2$ (crystalline phase, SII) to 21.5 Å$^2$ (*rotator* phase, SI). Moreover, taking into account the tilt angle of the chains with respect to the ionic layer (14°), the cross-sectional area of the alkyl chains ($S'$) can be calculated as $S' = S \cos 14°$. This yields a result of 20.8 Å$^2$ for the *rotator* phase of the lead(II) alkanoates. This value is similar to those found for *rotator* phases of *n*-alkanes (20 Å$^2$),[43] lithium *n*-hexadecanoate (20.7 Å$^2$),[44] lithium 16-hydroxy-

hexadecanoate (21.5 Å$^2$),[45] and Langmuir monolayers of alkyl chain surfactants in water (19.7−20.2 Å$^2$).[46,47] No definitive coordination number can be established for the lead(II) *rotator* phase. However, as shown by both FTIR and Pb-207 NMR techniques, a change in the lead(II) *hemidirected* coordination 6 of the crystal must occur in the *rotator* phase.

**Glass States and Kinetics.** The glass formation capability of the lead(II) alkanoates has recently been tested in the shortest members ($Pb(C2)_2$, $Pb(C3)_2$, and $Pb(C4)_2$).[11] Only the common vitreous state from the isotropic liquid is found in these compounds. $Pb(C5)_2$ maintains this tendency as a glass-former. However, as shown above, two different glass states are detected. To our knowledge, this is the first time that a *rotator glass* (GI) has been characterized. Thus, GI and GII correspond to the freezing of the *dynamic* disorder taking place in the *rotator* phase (SI) and isotropic liquid (IL), respectively. The values of $\Delta Cp$ for GII and GI are approximately 150 and 15 $J \cdot K^{-1} \cdot mol^{-1}$, respectively, in agreement with the big difference in nature of both types of glasses (a higher disordered structure of GII).

The values for both Tg's at different heating rates ($\alpha$) are displayed in Table 2. Two kinetic equations were applied to the data:

- Kissinger's equation:[48,49]

$$\ln\left(\frac{Tg^2}{\alpha}\right) = \frac{E_a}{R}\frac{1}{Tg} + C$$

- Ozawa's equation:[49,50]

$$\ln \alpha = \frac{E_a}{R}\frac{1}{Tg} + C$$

to determine the corresponding activation energy ($E_a$) of the glass transitions. This can also be calculated for the crystallization process. These equations work satisfactorily except for slow heating rates (Figure 12). The data of $E_a$ for Tg2, $T_{crys}$, and Tg1 obtained from the linear fits of both kinetic equations are reported in Table 4. The $E_a$ values are comparable to those found in poly(3-hydroxybutyrate)[51] or some alloys ($KSb_5S_8$, $Se_xTe_{100-x}$, $Se_xIn_{100-x}$, or $Bi_xSe_{100-x}$).[52−54] Obviously, no data were found for the glass transition involving a *rotator* phase (GI-to-SI).

We have no definitive explanation for the easy lead(II) pentanoate quenching into two different glass states. Conditions favoring vitrification are hindrance of the crystallization process or chemical incompatibility between the central core and flexible parts of the molecule.[55] In this regard, lead(II) alkanoates have a more hindered internal rotation of the methylene groups (smaller alkyl chain cross-sectional area ($S'$)) than other homologous alkanoates with monovalent cations, because they have double amount of alkyl chains.[56−59] On the other hand, from a chemical point of view, the central core of ionic layers is very different from the alkyl chains. Moreover, the lower and higher the melting and boiling points are, the easier is the formation of a glass state.[55] The lead(II) pentanoate melts at 355.6 K (*ionic liquid*) which is very low for an organic salt. According to this rule,[31] glass formation would be easy in this compound.

## 5. Conclusions

The thermal information reported here completes the study of the lead(II) alkanoates series, being the first time data for lead(II) pentanoate have been reported. $Pb(C5)_2$ shares properties of the shorter and longer members of the lead(II) alkanoates series, such as glass formation (as in the shorter) and the existence of an intermediate *rotator* phase (as in the longer), respectively.

The structure of the crystalline phase (SII) has been proven to be isostructural with the rest of the lead(II) alkanoates in the same phase. $Pb(C5)_2$ also shows the presence of a *rotator* phase (SI). In this respect, the transition from SII to SI is *polymorphic*, associated with an *order−disorder* change from the *herringbone* or *chevron* order (of the *all-trans* carbon planes) to a possible *six-fold* random disorder of the same planes in the *rotator* phase (as observed in lead(II) hexanoate to dodecanoate members). Apart from the existence of the *rotator* phase, the other main feature of $Pb(C5)_2$ is the formation of two *vitreous* states: one from this phase and another from the isotropic liquid. The calorimetric and spectroscopic analysis has shown the *regular* and *rotator* nature of these glass states. Moreover, the kinetic characteristic parameters of the vitrification process have been measured. The study of the behavior of this kind of compounds is also of great interest in the field of *step-wise melting* processes: transitions (solid-to-solid and/or melting) taking place from a totally ordered crystalline phase at low temperature to the isotropic liquid, typical of all of the organic families.

**Acknowledgment.** Partial support of this research by the DGICYT of the Spanish *Ministerio de Educación y Ciencia* (Project CTQ2007-668/7/BQU) is gratefully acknowledged. The authors wish to thank the CAI's (Centro de Asistencia a la Investigación) of XRD and Spectroscopy of the UCM for the use of their technical facilities.

## References and Notes

(1) Claudio, E. S.; Magyar, J. S.; Godwin, H. A. Fundamental Coordination Chemistry, Environmental Chemistry, and Biochemistry of Lead(II). *Prog. Inorg. Chem.* **2003**, *51*, 1–144.

(2) Harrowfield, J. *Helv. Chim. Acta* **2005**, *88*, 2430–2432.

(3) Bazuin, C. G.; Guillon, D.; Skoulios, A.; Amorim da Costa, A. M.; Burrows, H. D.; Geraldes, C. F. G. C.; Teixeira-Dias, J. J. C.; Blackmore, E.; Tiddy, G. J. T. *Liq. Cryst.* **1988**, *3* (12), 1655–1657.

(4) Schwede, J.; Koehler, L.; Grossmann, H. P.; Pietralla, M.; Burrows, H. D. *Liq. Cryst.* **1994**, *16* (2), 267–276.

(5) Ellis, H. A.; de Vries, J. W. C. *Mol. Cryst. Liq. Cryst.* **1988**, *163*, 133–139.

(6) Amorim da Costa, A. M.; Burrows, H. D.; Geraldes, C. F. C. G.; Teixeira-Dias, J. J. C.; Bazuin, C. G.; Guillon, D.; Skoulios, A.; Blackmore, E.; Tiddy, G. J. T.; Turner, D. L. *Liq. Cryst.* **1986**, *1* (3), 215–226.

(7) Sánchez Arenas, A.; García, M. V.; Redondo, M. I.; Cheda, J. A. R.; Roux, M. V.; Turrión, C. *Liq. Cryst.* **1995**, *18*, 431–441.

(8) Adeosun, S. A.; Sime, S. J. *Thermochim. Acta* **1978**, *27*, 319–327.

(9) Ekwunife, M. E.; Nwachukwu, M. U.; Rinehart, F. P.; Sime, S. *J. Chem. Soc., Faraday Trans. 1* **1975**, *71* (7), 1432–1446.

(10) Martínez Casado, F. J.; García Pérez, M. V.; Redondo Yélamos, M. I.; Cheda, J. A. R.; Sánchez Arenas, A.; López de Andrés, S.; García-Barriocanal, J.; Rivera, A.; León, C.; Santamaría, J. *J. Phys. Chem. C* **2007**, *111* (18), 6826–6831.

(11) Martínez-Casado, F. J.; Sánchez Arenas, A.; García Pérez, M. V.; Redondo Yélamos, M. I.; López de Andrés, S.; Cheda, J. A. R. *J. Chem. Thermodyn.* **2007**, *39* (3), 455–461.

(12) Duffy, J. A.; Ingram, M. D. *J. Am. Ceram. Soc.* **1969**, *52*, 224–225.

(13) Ingram, M. D.; Lewis, G. G.; Duffy, J. A. *J. Phys. Chem.* **1972**, *76* (7), 1035–1040.

(14) Bartholomew, R. F.; Lewek, S. S. *J. Am. Ceram. Soc.* **1970**, *56* (8), 445–447.

(15) Lacouture, F.; Francois, M.; Didierjean, C.; Rivera, J. P.; Rocca, E.; Steinmetza, J. *Acta Crystallogr.* **2001**, *C57*, 530–531.

(16) Wunderlich, B.; Möler, M.; Grebowicz, J.; Baur, H. In *Conformational Motion and Disorder in Low and High Molecular Mass Crystals*; Höcker, H., Ed.; Advances in Polymer Science, Number 87; Springer-Verlag: Heidelberg, Germany, 1988.

(17) Wunderlich, B. *Thermochim. Acta* **1999**, *37*, 340–341.

(18) Descamps, M.; Correia, N. T.; Derolled, P.; Danede, F.; Capet, F. *J. Phys. Chem. B* **2005**, *109* (33), 16092–16098.

(19) Collings, P. J.; Patel, J. S. *Handbook of Liquid Crystal Research*; Oxford University Press: New York, 1997.

(20) Habenschuss, A.; Varma-Nair, M.; Kwon, Y. K.; Ma, J.; Wunderlich, B. *Polymer* **2006**, *47* (7), 2369–2380.
(21) Parr, J. *Polyhedron* **1997**, *16* (4), 551–566.
(22) Seddon, K. R.; Stark, A.; Torres, M. J. *Pure Appl. Chem.* **2000**, *72* (12), 2275–2287.
(23) Holbrey, J. D.; Seddon, K. R. *Ionic Liq.* **1999**, *1*, 232–236.
(24) Ascenso, J. R.; Harris, R. K. *J. Organomet. Chem.* **1986**, *301*, C23–C26.
(25) Kurik, M. V.; Lavrentovich, O. D. *Sov. Phys. Usp.* **1988**, *31* (3), 196–224.
(26) Chapman, D. *Chem. Rev.* **1962**, *62* (5), 433–456.
(27) Maroncelli, M.; Qi, S. P.; Strauss, H. L.; Snyder, R. G. *J. Am. Chem. Soc.* **1982**, *104*, 6237–6247.
(28) Spitalsky, Z.; Bleha, T. *Macromol. Theory Simul.* **2001**, *10* (9), 833–841.
(29) Burrows, H. D.; Geraldes, F. G.C.; Pinheiro, T. J. T.; Harris, R. K.; Sebald, A. *Liq. Cryst.* **1988**, *3* (6−7), 853–860.
(30) Ryckaert, J. P.; Klein, M.; McDonald, I. R. *Mol. Phys.* **1994**, *83*, 439–458.
(31) Fujiwara, S.; Sato, T. *J. Chem. Phys.* **1999**, *110* (19), 9757–9764.
(32) Marbeuf, A.; Brown, R. *J. Chem. Phys.* **2006**, *124* (5), 054901/1-054901/9.
(33) Barman, S.; Venkataraman, N. V.; Vasudevan, S.; Seshadri, R. *J. Phys. Chem. B* **2003**, *107*, 1875–1883.
(34) Asayama, R.; Kawamura, J.; Hattori, T. *Chem. Phys. Lett.* **2005**, *414* (1−3), 87–91.
(35) Gray, G. W.; Goodby, J. W. *Smectic Liquid Crystals*, 1st ed.; Leonard Hill: London, 1984.
(36) Jaimez, E.; Slade, R. C. T. *J. Chem. Soc., Dalton Trans.* **1997**, *8*, 1435–1440.
(37) Vogel, A.; Katzka, C. P.; Waldmann, H.; Arnold, K.; Brown, M. F.; Huster, D. *J. Am. Chem. Soc.* **2005**, *127*, 12263–12272.
(38) Ryckaert, J. P.; McDonald, I. R.; Klein, M. L. *Mol. Phys.* **1989**, *67* (5), 957–979.
(39) Fujiwara, S.; Sato, T. *Prog. Theor. Phys. Suppl.* **2000**, *138*, 342–347.
(40) Adebahr, J.; Seeber, A. J.; MacFarlane, D. R.; Forsyth, M. A. *J. Appl. Phys.* **2005**, *97*, 093904−093905. *J. Phys. Chem. B* **2005**, *109*, 20087−20092.
(41) Busico, V.; Cernicchiaro, P.; Corradini, P.; Vacatello, M. *J. Phys. Chem.* **1983**, *87*, 1631–1635.
(42) Iwai, S.; Hattori, M.; Nakamura, I. D.; Ikeda, R. *J. Chem. Soc., Faraday Trans.* **1993**, *89* (5), 827–931.
(43) Strobl, G.; Ewen, B.; Fischer, E. W.; Piesczek, W. *J. Chem. Phys.* **1974**, *61* (12), 5257–5264.
(44) Busico, V.; Ferraro, A.; Vacatello, M. *J. Phys. Chem.* **1984**, *88* (18), 4055–4058.
(45) Busico, V.; Ferraro, A.; Vacatello, M. *J. Chem. Phys.* **1986**, *84* (1), 471–475.
(46) Sirota, E. B. *Langmuir* **1997**, *13* (14), 3849–3859.
(47) Vollhardt, D. *J. Phys. Chem. C* **2007**, *111* (8), 6805–6812.
(48) Kissinger, H. E. *J. Res. Natl. Bur. Stand. (U.S.)* **1956**, *57* (4), 217–221.
(49) Cheng, K. *Mater. Sci. Eng., B* **1999**, *60* (3), 194–199.
(50) Ozawa, T. *Bull. Chem. Soc. Jpn.* **1965**, *38* (11), 1881.
(51) Sha, W. *J. Appl. Polym. Sci.* **2001**, *80* (13), 2535–2537.
(52) Chrissafis, K.; Kyratsi, T.; Paraskevopoulos, K. M.; Kanatzidis, M. G. *Chem. Mater.* **2004**, *16* (10), 1932–1937.
(53) Mehta, N.; Kumar, A. *J. Optoelectron. Adv. Mater.* **2005**, *7* (3), 1473–1478.
(54) Moharram, A. H.; Abu El-Oyoun, M. *J. Phys. D: Appl. Phys.* **2000**, *33* (6), 700–703.
(55) Debenedetti, P. G. *Metastable Liquids*; Princeton University Press: Princeton, NJ, 1996.
(56) Cheda, J. A. R.; Redondo, M. I.; García, M. V.; López de la Fuente, F. L.; Fernandez-Martín, F.; Westrum, E. F., Jr. *J. Chem. Phys.* **1999**, *111*, 3590–3598.
(57) Binnemans, K. *Chem. Rev.* **2005**, *105*, 4148–4204.
(58) Mirnaya, T. A.; Volkov, S. V. Ionic Liquid Crystals as Universal Matrices (Solvents). Main Criteria for Ionic Mesogenicity. In *Green Industrial Applications of Ionic Liquids*; Rogers, R. D., Seddon, K. R., Volkov, S., Eds.; NATO Science Series; Kluwer Academic Publ: Dordrecht, The Netherlands, 2003; pp 439−456.
(59) Franzosini, P.; Sanesi, M., Eds. *Thermodynamic and transport properties of organic salts*; Pergamon Press: Oxford, U.K., 1980.

JP804757N